Subtracting tilt from a horizontal-seismometer using a ground-rotation-sensor

Krishna Venkateswara[1], Charles A. Hagedorn, Jens H. Gundlach

University of Washington, Seattle WA USA

Jeffery Kissel, Jim Warner, Hugh Radkins, Thomas Shaffer

LIGO Laboratory, Hanford WA USA

Brian Lantz

Stanford University, Stanford CA USA

Richard Mittleman, Fabrice Matichard

MIT, Cambridge MA USA

Robert Schofield

University of Oregon, Eugene OR USA

ABSTRACT We demonstrate the use of a high-precision ground-rotation-sensor to subtract wind induced tilt noise in a horizontal broadband seismometer at frequencies above 10 mHz. The measurement was carried out at the LIGO Hanford Observatory using a low-frequency

[1] kvenk@uw.edu

flexure-beam-balance with an autocollimator readout and a T240 seismometer, located in close proximity to each other. Along their common horizontal axis, the two instruments show significant coherence below 100 mHz, which increases as a function of wind speed due to floor tilt induced by wind pressure on the walls of the building and the ground outside. Under wind speeds of 10-15 m/s, correcting the seismometer for measured ground-rotation lowered the signal by a factor of ~10 between 10-100 mHz. This paper describes the instruments used, shows representative data for low and high wind speeds, and discusses the tilt-subtraction and possible limitations.

INTRODUCTION

The inability to distinguish between time-varying horizontal displacement and slow rotation (tilt) by seismometers has been a long standing problem in seismology (**Rodgers (1968), Lee *et al*. (2009), De Angelis and Bodin (2012)**) with important ramifications in active seismic isolation (**Lantz *et al*. (2009)**). This is because seismometers are essentially acceleration sensors and a horizontal acceleration sensor alone is insufficient to distinguish between the two sources of acceleration - acceleration from horizontal translation or that due to gravity coupling through rotation. Ordinary tiltmeters, such as simple pendulums or spirit levels, also suffer from the same problem since they gauge tilt by comparing horizontal acceleration to the vertical (at frequencies below their resonances).

In this paper, we define ‘tilt’ of the ground as its angle with respect to the horizontal axis of a nearly inertial frame fixed to the local gravitational vertical (defined by a free-falling mass). This frame is not strictly inertial, because of changes in local gravity and Earth's rotation. However,

these effects are small in the frequency region under discussion (above 10 mHz) and are ignored here.

The apparent displacement x as interpreted by a seismometer due to a tilt θ at angular frequency $\omega = 2\pi f$ is given by

$$|x| = \frac{g}{\omega^2}|\theta| \quad (1)$$

where g is the acceleration due to gravity. Due to the ω^2 in the denominator, response to tilt can often dominate seismometer output below 100 mHz.

One way to separate displacement and rotation is to measure tilt/rotation (with respect to the inertial frame) using beam-balances (see **Robertson *et al*. (1982)**, **Speake and Newell (1990)**) or through other means such as ring-laser-gyroscopes (see **Belfi *et al*. (2012)**). This independent sensor can then be used to subtract the tilt component from a seismometer's output to provide a pure displacement output. If the sensors measured identical signals, the subtraction would be limited only by the noise in the two sensors. However, in practice since the sensors are separated by some distance, the subtraction could be limited by the difference in tilt between the two locations. Mechanical filtering of the tilt transmission to a seismometer is an interesting alternative technique of measuring tilt-free horizontal displacement (**Matichard *et al*. (2015)**) as compared to direct tilt measurement and subtraction.

We demonstrate tilt-subtraction using a low-frequency beam-balance whose angle is measured using a high-sensitivity autocollimator. Two such rotation sensors were built at the University of Washington, Seattle (UW). The main features and performance of the first sensor are summarized in **Venkateswara *et al*. (2014)**. The second sensor was built and tested at UW and subsequently installed at the LIGO Hanford Observatory (LHO), where tilt motion currently

limits the performance of the active isolation platforms at low frequency (**Matichard, Lantz *et al*. (2015)**). This second instrument is referred to as the Beam-Rotation-Sensor (BRS). The requirement for a ground rotation sensor to improve the active seismic isolation in Advanced LIGO (**Aasi, J *et al.* (2015)**) is described in **Lantz *et al.* (2009).**

Discussion of other tiltmeters: In the last three decades, several sensitive rotation-sensors have been proposed or built (see **Matichard and Evans (2015)** for a review of the field). **Speake and Newell (1990)** developed a tiltmeter based on a dumbbell suspended by crossed-flexures near its center of mass, establishing limits of 1 nrad/$\sqrt{(\text{Hz})}$ between 3-10 Hz. **Winterflood *et. al*. (2000)** developed a tilt sensor composed of a bar suspended by a metallic glass flexure with a shadow-sensor readout with a reported sensitivity of 0.2 nrad/$\sqrt{(\text{Hz})}$ above 1 Hz. More recently, **Dergachev *et al*. (2014)** developed a tilt sensor consisting of a beam-balance suspended by two knife-edges and an air-core LVDT readout. They report a tilt sensitivity of 5.7 nrad/$\sqrt{(\text{Hz})}$ sensitivity at 10 mHz and 0.64 nrad/$\sqrt{(\text{Hz})}$ above 100 mHz.

Vertically oriented Ring Laser Gyroscopes can also be very sensitive tiltmeters (**Korth *et al*. (2015), Schreiber and Wells (2013)**). **Belfi *et al*. (2012)**, report on a 1.82-m^2 ring laser gyro with sensitivity of 3 nrad/$\sqrt{(\text{Hz})}$ at 100 mHz and better than 0.1 nrad/$\sqrt{(\text{Hz})}$ above 3 Hz.

DESCRIPTION OF THE INSTRUMENTS

The BRS consists of a 0.86-m beam-balance, suspended by two Beryllium-Copper flexures. Its angle is measured with respect to a reference mirror using a differential autocollimator described in **Arp et al. (2014)**. The reference mirror is a beam-splitter mounted rigidly with respect to the ground and in the same optical path as the target mirror on the beam-balance. Measurement of

the beam-balance angle relative to the reference mirror allows for subtraction of any common-mode noise, such as thermal drift of the autocollimator body. As suspended, the resonant frequency of the beam-balance is 8.79 mHz, moment of inertia of 0.59-kg-m^2 and the mechanical quality factor is 4.8×10^3. It is placed in a vacuum vessel which is pumped down to pressures of less than 10^{-4} Pa by an ion pump.

A detailed discussion of the tilt and acceleration-sensitivity of a beam-balance, such as the BRS is given in **Venkateswara et al. (2014)**. A schematic of the BRS with relevant angles is shown in Figure 1. When the ground tilts at frequencies above the BRS resonance frequency, the balance tends to stay fixed w.r.t. the inertial frame, thus the autocollimator measures the ground rotation w.r.t. the inertial frame (inertial-tilt). If the center of mass of the balance is located at the pivot/suspension point, then ground acceleration applies no torque on the balance. Detailed discussion of the dynamics is given in Appendix A. Appendix B describes a measurement of the translational sensitivity of such a device.

The suspension frame of the beam-balance is firmly clamped to the base of a vacuum vessel, which in turn was secured to a 2.5-cm thick and 0.9-m by 0.6-m aluminum plate. The three feet of this plate rest on the concrete floor of the X-End-station of the LIGO Hanford Observatory. The foundation is approximately 0.8-m-thick. Small rubber shims, roughly 3-mm-thick, were placed under the feet of the BRS-plate to isolate it from any high-frequency vibration. The entire apparatus, including the baseplate, is enclosed in a 5-cm-thick rigid-foam enclosure which provides passive thermal insulation and shielding from air flows. The hall is temperature controlled to roughly +/- 0.5 deg C.

The seismometer used for this study was a Nanometrics Trillium 240 Broadband Sensor. It was located about 1 m away from the center of the BRS. It also has three feet which rest on the same floor and has a separate thermal enclosure.

A cup anemometer (part of a Davis Weather Station-II), mounted to the roof of the End-station, is used to record wind-speed and direction.

DATA AT HIGH WIND-SPEEDS

Figure 2 shows the amplitude spectral density (ASD) of data taken with the BRS during a windy period. The data were taken for 5000 seconds on May 16 2015 from 3:20 to 4:43 UTC for the ASD, which was calculated using the periodogram method and averaged over five frequency bins. Figure 3 shows the wind-speed, the BRS tilt output, the T240 velocity output and the tilt-corrected velocity as a function of time. The last three signals were high-passed using a 10 mHz, 4^{th} order Butterworth filter to suppress lower-frequency content. The wind speeds were roughly between 10 and 15 m/s. The tilt-subtraction procedure is described below.

The raw angular position (autocollimator output) of the BRS is labelled simply as 'BRS angle' ($\boldsymbol{\theta_a}$). The resonance of the beam-balance is visible at 8.9 mHz. The peak visible at 3.1 Hz is due to the torsional mode of the balance, coupling in through small asymmetries in the angular readout. Also shown is the 'BRS ref' signal, the angular motion of the reference mirror used in the BRS autocollimator. As the autocollimator output is the difference in angle between the mirror on the beam-balance and the reference mirror, BRS ref can be interpreted as $1/\sqrt{2}$ times the upper limit of the angle readout noise. Any common-noise (such as thermal drifts) between

the two is subtracted while other noise (such as electronic noise) adds incoherently, increasing the total by a factor of $\sqrt{2}$.

The horizontal acceleration,a_x, as measured by the T240 seismometer located close to the BRS will be influenced by both horizontal displacement of the ground and ground tilt. Ideally if the separation between the center of mass (COM) and the suspension point/pivot of the beam-balance ('d') were negligibly small, then the BRS would be sensitive only to ground tilt. However, due to a small but finite 'd', BRS output is also influenced to a small extent by horizontal acceleration and this must be corrected in order to separate the two. To convert the autocollimator measured angle of the BRS to ground tilt, we use the following equation (derived in Appendix A) in frequency space:

$$\theta_p = -\frac{\omega^2 - \omega_0^2(1+i\varphi)}{\omega^2}\theta_a + \frac{Md}{I\omega^2}a_x \qquad (2)$$

where θ_p is the ground tilt at angular frequencyω, ω_0 is the resonant frequency, φ is the internal loss factor of the flexure, I is the moment of inertia (0.59 kg-m^2), M is the total mass (4.2 kg), and d is the separation between the center of mass (COM) and the suspension point/pivot of the beam-balance, and a_x is the horizontal acceleration measured by the T240.

The result of the ground-tilt computation is shown in Figure 4. The first term on the right-hand-side in Eq. (2) is the inversion of the ideal beam-balance response (labelled as 'Ground-tilt according to BRS') and the second is an acceleration-response correction (labelled as 'Correction using T240') due to a small but finite 'd', separately measured to be (33+/-5) μm. Alternatively, 'd' could be extracted by fitting the low-frequency part of the BRS and T240 data which yields the same value of d. The acceleration correction is only important at frequencies near 20 mHz

and below as seen from the plot. To show the readout-noise contribution, we also apply the first term in Eq. (2) to the BRS ref data ($\times \sqrt{2}$), labelled as 'BRS readout noise contribution'.

The computed ground-tilt can then be converted into acceleration units by multiplying by the acceleration due to gravity, g, and then subtracting it from the measured acceleration as shown in Figure 5. The plot shows the ASD of the T240 acceleration, the corrected ground-tilt contribution and the tilt-subtracted residual. The frequency response of the T240 instrument has been compensated. The residual horizontal acceleration is smaller than the seismometer amplitude between 6 to 90 mHz by factors of 2-10. The BRS noise contribution, computed as g times the BRS ref noise contribution, is also shown.

There are several noteworthy features in Figure 5. Although the microseismic amplitude was relatively small during this period, it is interesting to note that even at 0.2 Hz, tilt accounts for one-fifth of the horizontal acceleration measured by the seismometer. The average ground rotation spectral density is relatively smooth at low frequencies but falls off quickly above ~300 mHz.

At frequencies above 100 mHz, the acceleration residual matches the T240 acceleration, while the BRS curve is much smaller, demonstrating that the two sensors measure different quantities. This becomes more evident when wind-speeds are low as shown in the next section. Going from right to left in frequency, between 100 to 35 mHz, it decreases as nearly f^2, but below 30 mHz, it goes as $1/f^2$. If the tilt-subtraction were limited only by the BRS readout noise, one would expect the f^2-trend to continue until it intersects the BRS noise contribution curve and to then follow that curve. This deviation indicates an excess noise contribution at low frequencies, discussed in subsequent sections. Figure 6 shows a plot of the transfer function between

translation measured by the seismometer and the tilt measured by BRS. Also shown are two straight line fits to the data at low and high frequencies. At low frequencies, the translation has the expected $\boldsymbol{g/\omega^2}$ dependence. At frequencies near 1000 mHz, the translation appears to be proportional to the tilt, indicating rotation about a pivot ~ 10 meters underground. If this relation were to hold down to 10 mHz, the wind-induced horizontal acceleration ASD would be ~ 2 nm/s^2/$\sqrt{(\mathbf{Hz})}$. This is far too small to explain the excess noise in the acceleration residual.

The first plot in Figure 7 shows the coherence between the T240 and BRS data and between the sensors and the residual acceleration. The low coherence for the latter two curves shows that the subtraction removes most of the common (tilt) signal between the two instruments. The second plot in Figure 7 is an estimate of the expected subtraction factor based on the observed coherence, calculated as

$$sub.factor = \frac{1}{\sqrt{1 - coherence}} \tag{3}$$

The ratio of the T240 acceleration to the residual acceleration is shown, which agrees well with the expected subtraction factor. The slight decrease in the ratio near 100 mHz is due to the extra coherence between the two instruments caused by the direct rotation to translation coupling discussed above and shown in Figure 6. As the goal is to measure the inertial translation of the ground, we do not subtract this direct coupling, resulting in the reduced subtraction factor.

Figure 8 shows the ASD of data taken with the BRS and a T240 seismometer during another windy period. The data were taken for 5000 seconds on October 12, 2014, from 00:45 to 2:09 UTC and the ASD was calculated as before. As before, Figure 9 shows the wind speeds, which were mostly between 10 and 15 m/s and also shows the BRS output, and the T240 velocity output before and after tilt-subtraction. Also shown in Figure 8 is a second T240 acceleration

spectrum measured about 3 hours later when wind speeds were lower. In this case, it is particularly interesting to note that the high-wind seismometer spectrum is swamped by tilt-noise below 0.1 Hz and cannot resolve the primary microseismic peak. But after, tilt-subtraction, the peak is distinct and this peak height matches with that measured 3 hours later. As the primary microseismic peak height varies only slowly with time, this indicates that the acceleration residual is indeed mainly composed of acceleration from horizontal ground displacement.

DATA AT LOW WIND-SPEEDS

Figure (10) shows a similar tilt-subtraction for low wind-speed data, as measured with the BRS and the T240 seismometer. The data were taken for 5000 seconds on May 14, 2015 from 02:00 to 03:23 UTC. As before, Figure 11 shows the relevant times-series data.

In Figure 10, the measured ground tilt is limited by the BRS noise above ~60 mHz. Below that, BRS measures a rising background which separates from the noise. The BRS noise looks nearly identical to that in the previous cases indicating that the intrinsic noise of the autocollimator is unchanged between the two cases. The acceleration residual is dominated by the T240 acceleration above 30 mHz. This plot also highlights the low translational sensitivity of the BRS. The curves diverge significantly at frequencies above 30 mHz. At 160 mHz, the T240 records an acceleration ASD of ~ 0.5 $\mu m/s^2/\sqrt{(Hz)}$ or a translation ASD of 0.5 $\mu m/\sqrt{(Hz)}$. The BRS however, shows a rotation-induced acceleration ASD of 0.003 $\mu m/s^2/\sqrt{(Hz)}$ or a tilt ASD of ~0.3 $nrad/\sqrt{(Hz)}$. The rotational component of microseismic-motion can be approximately estimated as $\sim \frac{2\pi X}{\lambda} = \frac{2\pi X \times f}{V}$, where X is the horizontal displacement amplitude, λ is the wavelength of the surface waves, V is the phase velocity and f is the frequency of the wave.

Estimating the phase velocity as ~3000 m/s, this implies a rotation signal ASD of 0.2 nrad/$\sqrt{(\mathrm{Hz})}$. This implies that the acceleration recorded by the T240 is dominated by translational motion of the ground and it shows a translation rejection in BRS of at least 6×10^{-4} rad/m or an acceleration rejection of 6×10^{-3} in dimensionless units at 160 mHz.

It is also interesting to note that the increase in ground rotation is nearly a factor of 100 in the 20-100 mHz range between Figure 5 and Figure 10, whereas the average increase in wind-speed is only a factor of ~10, indicating a strongly non-linear relation between the two. The drag force in air is proportional to the square of the flow velocity, which qualitatively agrees with the above observation.

DISCUSSION OF TILT-SUBTRACTED ACCELERATION RESIDUAL

From our experiments, it is clear that ground tilt can be measured and subtracted effectively from horizontal acceleration measurements. Under high-wind conditions, the tilt-subtracted residual acceleration is significantly lower than the seismometer output above 10 mHz but not as low as the residual under low-wind conditions, as one might expect if the same signal was being measured by the two instruments. Figure 12 shows an ASD of the tilt-subtracted residuals for the quiet case and the windy case along with the expected readout noise contribution. Based on Figure 6 and the discussion in the previous section, it is likely not due to increase in ground translation. Recent measurements made by placing a second seismometer on the floor at various distances from the first seismometer show that the tilt varies substantially over the floor. This suggests that the increase in the tilt residual arises from the small differences in tilt seen by the

BRS and the seismometer. Further improvement in subtraction could likely be achieved by placing both instruments on a common platform.

CONCLUSION

Tilt-subtraction from a horizontal seismometer has been demonstrated using a ground-rotation sensor located ~1 m away. The rotation-sensor consists of a flexure-suspended beam-balance with an autocollimator readout with intrinsic sensitivity of 0.15 nrad/$\sqrt{(\mathrm{Hz})}$ above 100 mHz. This instrument meets the requirement for a ground rotation sensor to improve Advanced LIGO described in **Lantz et al. (2009)**. A tilt-subtraction factor of 10 is achieved at 30 mHz under wind-speeds of 10-15 m/s.

DATA AND RESOURCES

Data used in this study were collected at the LIGO Hanford Observatory. It is available for download at: https://dcc.ligo.org/P1500278/Public/.

ACKNOWLEDGEMENTS

This work was carried out at the LIGO Hanford Observatory by members of LIGO laboratory, and the LIGO Scientific Council including University of Washington, Seattle, Stanford University and University of Oregon. LIGO was constructed by the California Institute of Technology and Massachusetts Institute of Technology with funding from the National Science Foundation (NSF), and operates under cooperative agreement PHY-0757058. Advanced LIGO was built under award PHY-0823459. This document has been assigned LIGO Laboratory document number LIGO-P1500278. The University of Washington, Seattle participation was

supported by funding from NSF under award PHY – 1306613. The authors would like to thank LIGO Hanford Observatory staff for their assistance with the installation and maintenance of the sensors. The authors are grateful for useful comments and suggestions by Ryan DeRosa, and Paul Bodin.

REFERENCES

Aasi, J., B. P. Abbott, R. Abbott, T. Abbott, M. R. Abernathy, K. Ackley, C. Adams, T. Adams, P. Adesso, R. X. Adhikari *et. al.*(2015). Advanced LIGO, *Class. Quantum Grav.* **32** 074001.

Arp, T. B., C. A. Hagedorn, S. Schlamminger, and J. H. Gundlach (2013). A reference-beam autocollimator with nanoradian sensitivity from mHz to kHz and dynamic range of 10^7. *Rev. Sci. Instrum.* **84**, 095007.

De Angelis, S and P. Bodin (2012). Watching the Wind: Seismic Data Contamination at Long Periods due to Atmospheric Pressure-Field-Induced Tilting. *Bull. Seismol. Soc. Am.* **102**, no. 3, 1255–1265, doi: 10.1785/0120110186.

Dergachev, V., R. DeSalvo, M. Asadoor, A. Bhawal, P. Gong, C. Kim, A. Lottarini, Y. Minenkov, C. Murphy, A. O'Toole, et al. (2014). A high precision, compact electromechanical ground rotation sensor. *Rev. Sci. Instrum.* **85**, no. 5, 054502, doi: 10.1063/1.4875375.

W. Z. Korth, A. Heptonstall, E. D. Hall, K. Arai, E. K. Gustafson, and R. X. Adhikari (2016). Passive, free-space laser gyroscope, *Class. Quantum Grav.* **33**, 035004.

Lantz, B., R. Schofield, B. O'Reilly, D. E. Clark, and D. DeBra (2009). Review: Requirements for a ground rotation sensor to improve Advanced LIGO. *Bull. Seismol. Soc. Am.* **99**, no. 2B, 980–989.

Lee,W. K., M. Celebi, M. I. Todorovska, and H. Igel, (2009). Introduction to the special issue on rotational seismology and engineering applications. *Bull. Seismol. Soc. Am.* **99**, no. 2B, 945–957.

Matichard, F. and M. Evans (2015). Review: Tilt-Free Low Noise Seismometry. *Bull. Seismol. Soc. Am.* **105**, no. 2A, 497–510.

Matichard, F., M. Evans, R. Mittleman, M. McInnis, S. Biscans, K.L. Dooley, H. Sohier, A. Lauriero, H. Paris, J. Koch e*t al.* (2016), Modeling and Experiment of the Suspended Seismometer Concept for Attenuating the Contribution of Tilt Motion in Horizontal Measurements. *Rev. Sci. Instrum.* **87**, no. 6, 065002.

Matichard, F., B. Lantz, R. Mittleman, K. Mason, J. Kissel, B. Abbott, S. Biscans, J. McIver, R. Abbott, S. Abbott, *et. al*. (2015). Seismic isolation of Advanced LIGO: Review of strategy, instrumentation and performance, *Class. Quantum Grav.* **32,** 185003.

O'Toole, A., F. E. Pena Arellano, A. V. Rodionov, M. Shaner, E. Sobacchi, V. Dergachev, R. DeSalvo, M. Asadoor, A. Bhawal, P. Gong, *et. al.* (2014). Deign and Initial characterization of a

compact ultra-high vacuum compatible low frequency tilt accelerometer. *Rev. Sci. Instrum.* **85**, 075003, doi: 10.1063/1.4890285.

Robertson, N. A., R. W. Drever, I. Kerr, and J. Hough (1982). Passive and active seismic isolation for gravitational radiation detectors and other instruments, *J. Phys. Sci. Instrum.* **15**, no. 10, 1101

Rodgers, P. W. (1968). The response of the horizontal pendulum seismometer to Rayleigh and Love waves, tilt, and free oscillations of the Earth. *Bull. Seismol. Soc. Am.* **58**, no. 5, 1385–1406.

Schreiber, K. U., and J. P. R. Wells (2013). Invited review article: Large ring lasers for rotation sensing. *Rev. Sci. Instrum.* **84**, no. 4, 041101.

Speake, C. C., and D. B. Newell (1990). *Rev. Sci. Instrum.* **61**, 1500.

Venkateswara, K., C. A. Hagedorn, M. D. Turner, T. Arp, and J. H. Gundlach (2014). A high precision mechanical absolute-rotation sensor. *Rev. Sci. Instrum.* **85**, no. 1, 015005, doi: 10.1063/1.4862816.

Winterflood, J., Z. B. Zhou, L. Ju, and D. G. Blair (2000), Tilt suppression for ultra-low residual motion vibration isolation in gravitational wave detection, *Phys. Lett. A* **277**, no. 3, 143–155.

Full mailing address of each author

Krishna Venkateswara (kvenk@uw.edu)

Charlie Hagedorn (cah49@uw.edu)

Jens Gundlach (jens@phys.washington.edu)

180, North Physics Lab bldg.,

CENPA, Box 354290

Seattle, WA 98195 USA

Jeff Kissel (jkissel@ligo.mit.edu)

Jim Warner (warner_j@ligo-wa.caltech.edu)

Hugh Radkins (radkins_h@ligo-wa.caltech.edu)

Thomas Shaffer (Shaffer_t@ligo-wa.caltech.edu)

LIGO Hanford Observatory

127124 N Route 10,

Richland WA 99354 USA

Brian Lantz (blantz@stanford.edu)

Richard Mittleman (richard@ligo.mit.edu)

Fabrice Matichard (fabrice@ligo.mit.edu)

LIGO Project MIT

MIT NW22-295

185 Albany street

Cambridge MA 02139 USA

Robert Schofield (rmssrmss@gmail.com)

List of Figure Captions

Figure 1: Schematic of the beam-balance. $\boldsymbol{\theta_p}$ is the angle of the ground w.r.t. a local inertial frame, $\boldsymbol{\theta_i}$ is the angle of the beam-balance w.r.t. the inertial frame and $\boldsymbol{\theta_a = \theta_i - \theta_p}$ is the angle measured by the autocollimator.

Figure 2: BRS raw angle measurement during high-winds. The solid curve is the angle of the beam-balance as measured by the autocollimator. The dashed curve is a measure of the autocollimator self-noise.

Figure 3: Time series of the wind-speed, BRS output and the T240 velocity from May 16 2015 starting at 3:20:00 UTC.

Figure 4: Ground tilt computation using the BRS and the T240. The ground tilt measured with BRS (solid) is corrected for finite acceleration coupling using the T240 (dashed) yielding the dotted curve. Also shown is the autocollimator noise contribution (dash-dot).

Figure 5: Tilt-subtraction in T240 acceleration data taken under windy conditions on May 16 2015. The tilt-subtracted residual acceleration is significantly smaller than the measured acceleration between 10-100 mHz.

Figure 6: Tilt to Translation transfer function. This plot shows the relation between the translation measured by the seismometer and the tilt measured by BRS. It has the expected $\boldsymbol{g/\omega^2}$ relation at low-frequencies but also shows a linear dependence at higher frequencies.

Figure 7: Coherence between T240, BRS and acceleration residuals, and the expected and measured subtraction factors.

Figure 8: ASD and coherence of data under windy conditions on October 11 2014. The primary microseismic peak is visible after tilt-subtraction and is a consistent height over time.

Figure 9: Time-series data from October 11 2014, starting at 00:45:00 UTC, showing a second high-wind duration.

Figure 10: ASD and coherence of data during low wind-speeds on May 14 2015.

Figure 11: Time series data from May 14 2015, starting at 02:00:00 UTC, showing a low-wind duration.

Figure 12: BRS readout noise contribution compared to the Lantz et. al. (2009) requirement. Also shown are the tilt-subtracted residual accelerations during low-wind and high-wind periods, converted to tilt units by dividing by g.

Figures

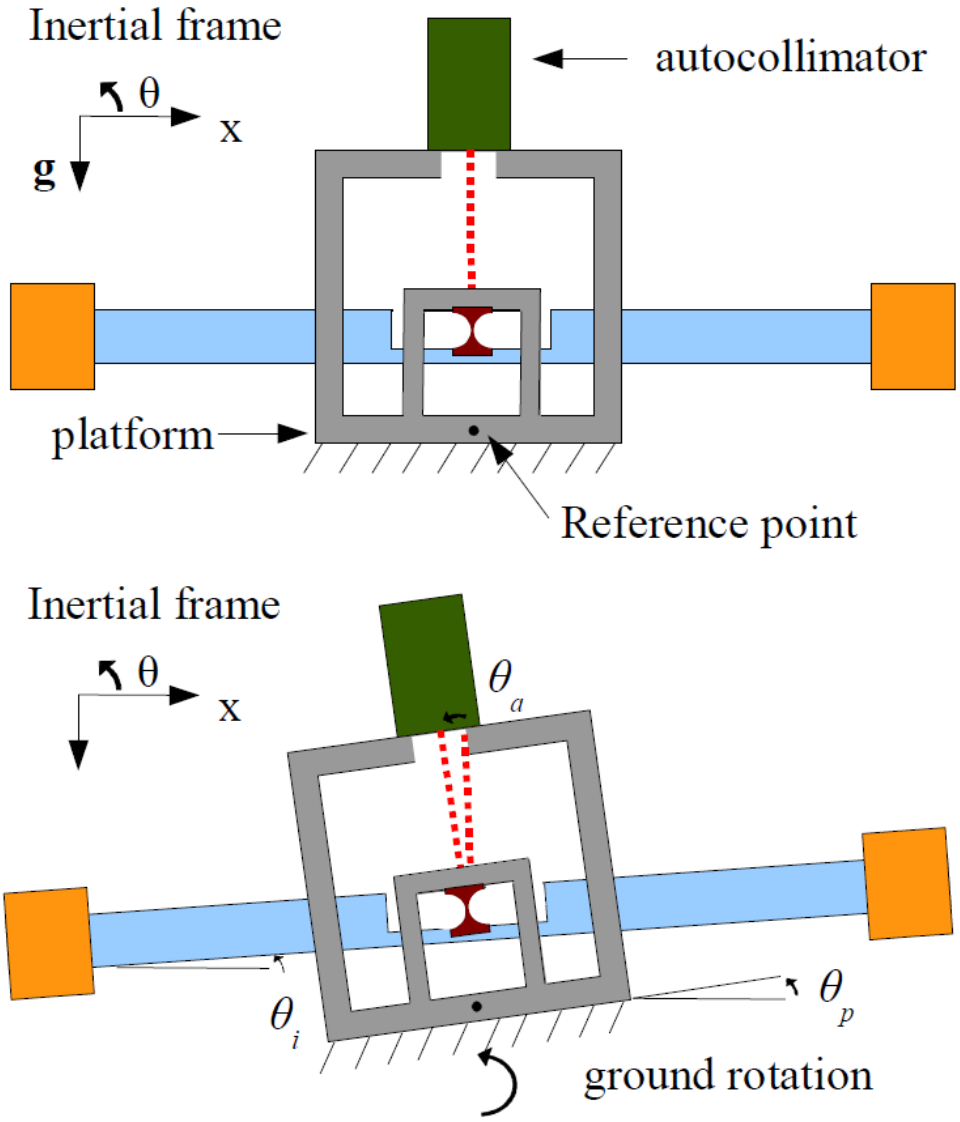

Figure 1: Schematic of the beam-balance. θ_p is the angle of the ground w.r.t. a local inertial frame, θ_i is the angle of the beam-balance w.r.t. the inertial frame and $\theta_a = \theta_i - \theta_p$ is the angle measured by the autocollimator.

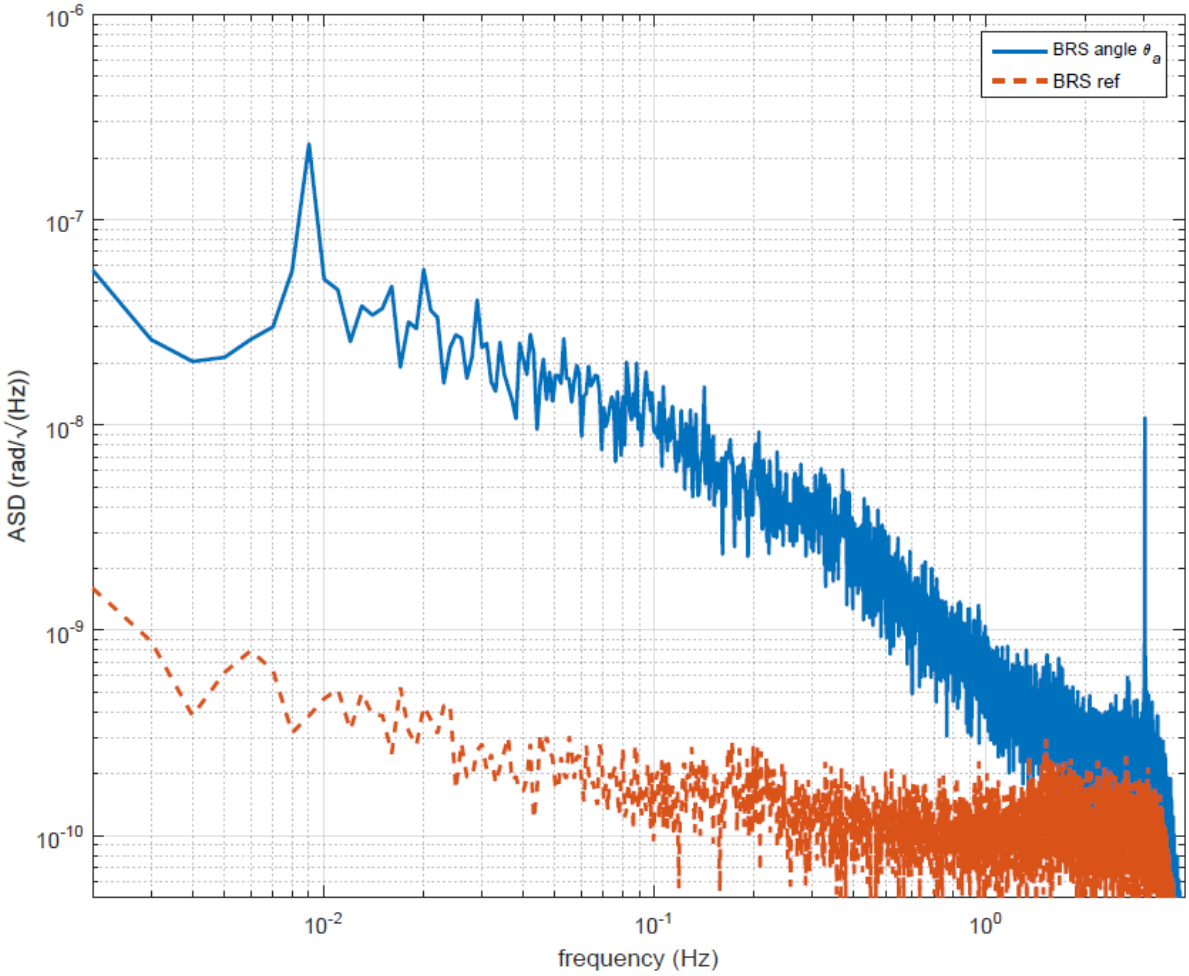

Figure 2: BRS raw angle measurement during high-winds. The solid curve is the angle of the beam-balance as measured by the autocollimator. The dashed curve is a measure of the autocollimator self-noise.

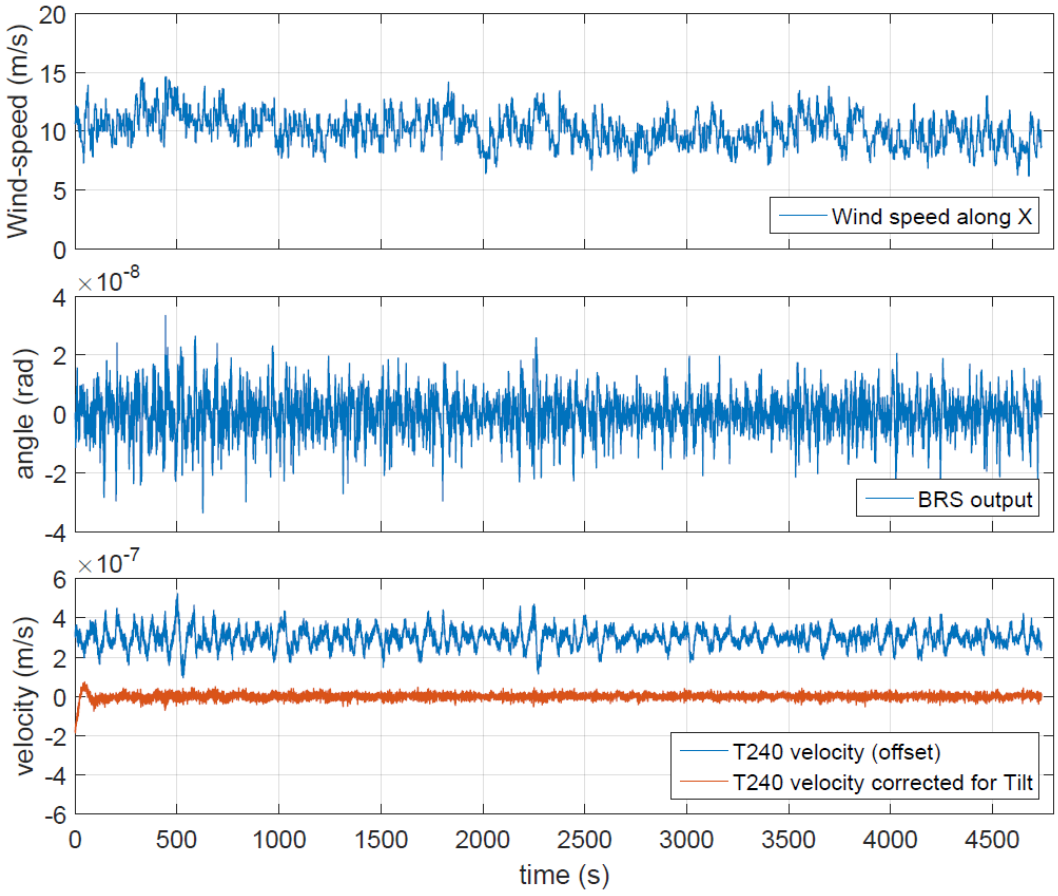

Figure 3: Time series of the wind-speed, BRS output and the T240 velocity from May 16 2015 starting at 3:20:00 UTC. Also shown is the T240 velocity after tilt correction. The data in the lower two panels have been high-passed with a 4th-order Butterworth filter.

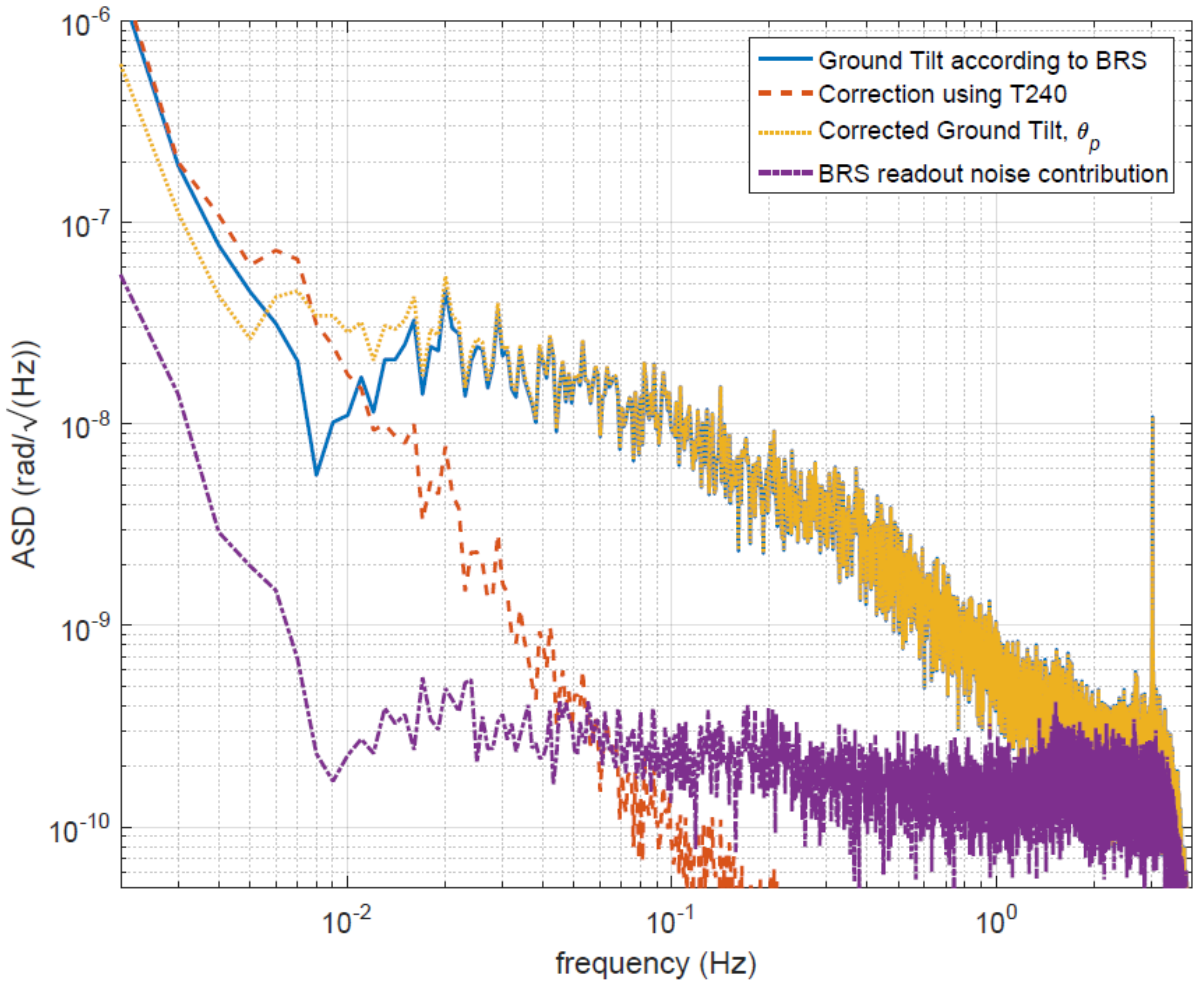

Figure 4: Ground tilt computation using the BRS and the T240. The ground tilt measured with BRS (solid) is corrected for finite acceleration coupling using the T240 (dashed) yielding the dotted curve. Also shown is the autocollimator noise contribution (dash-dot).

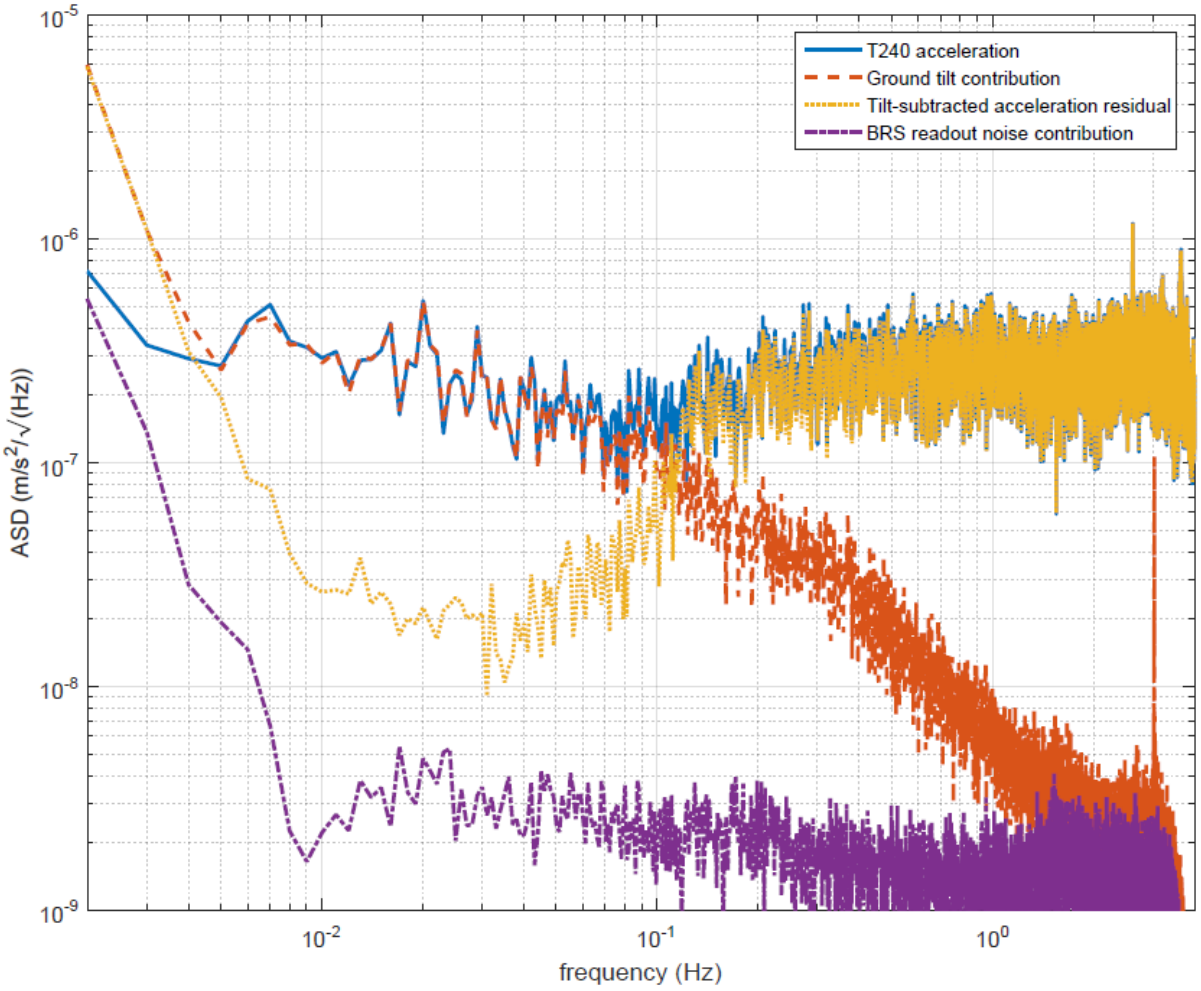

386

387 **Figure 5: Tilt-subtraction in T240 acceleration data taken under windy conditions on May**

388 **16 2015. The tilt-subtracted residual acceleration is significantly smaller than the measured**

389 **acceleration between 10-100 mHz.**

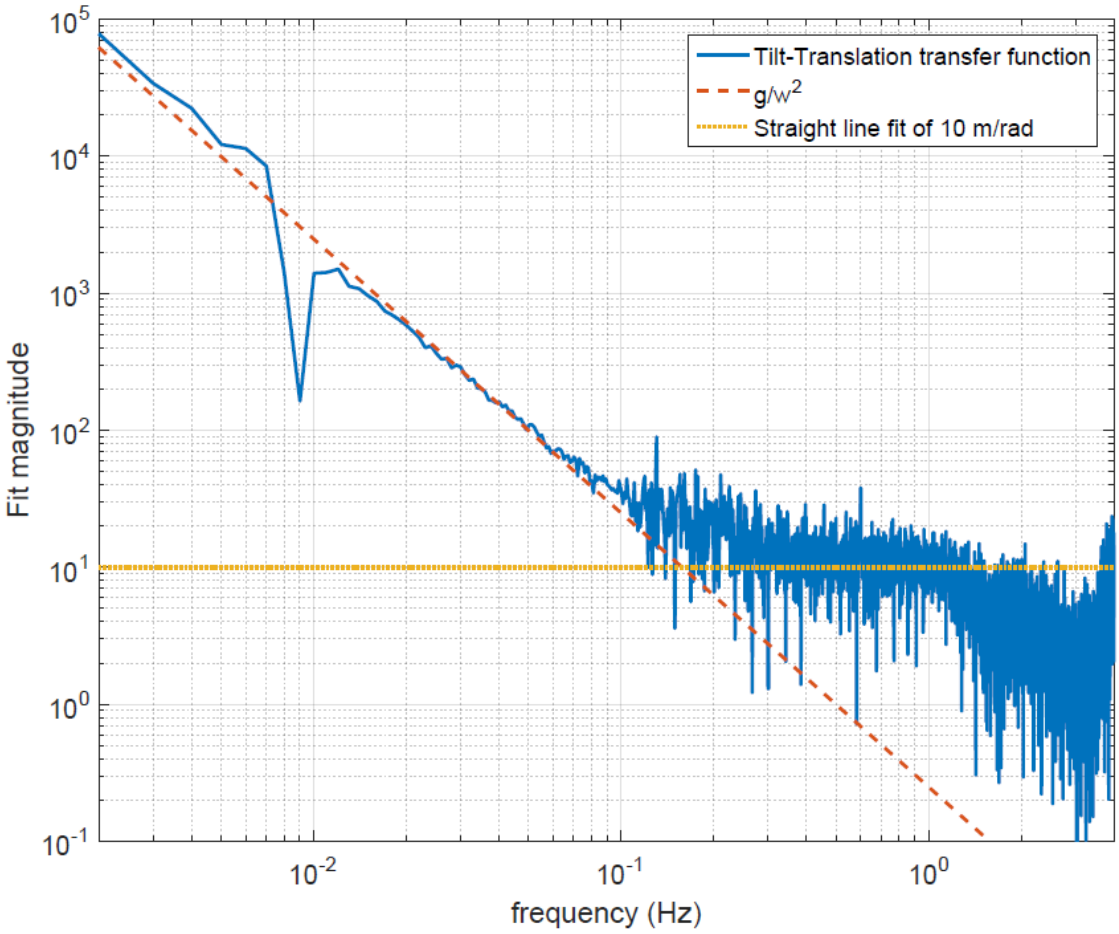

Figure 6: Tilt to Translation transfer function. This plot shows the relation between the translation measured by the seismometer and the tilt measured by BRS. It has the expected g/ω^2 relation at low-frequencies but also shows a linear dependence at higher frequencies.

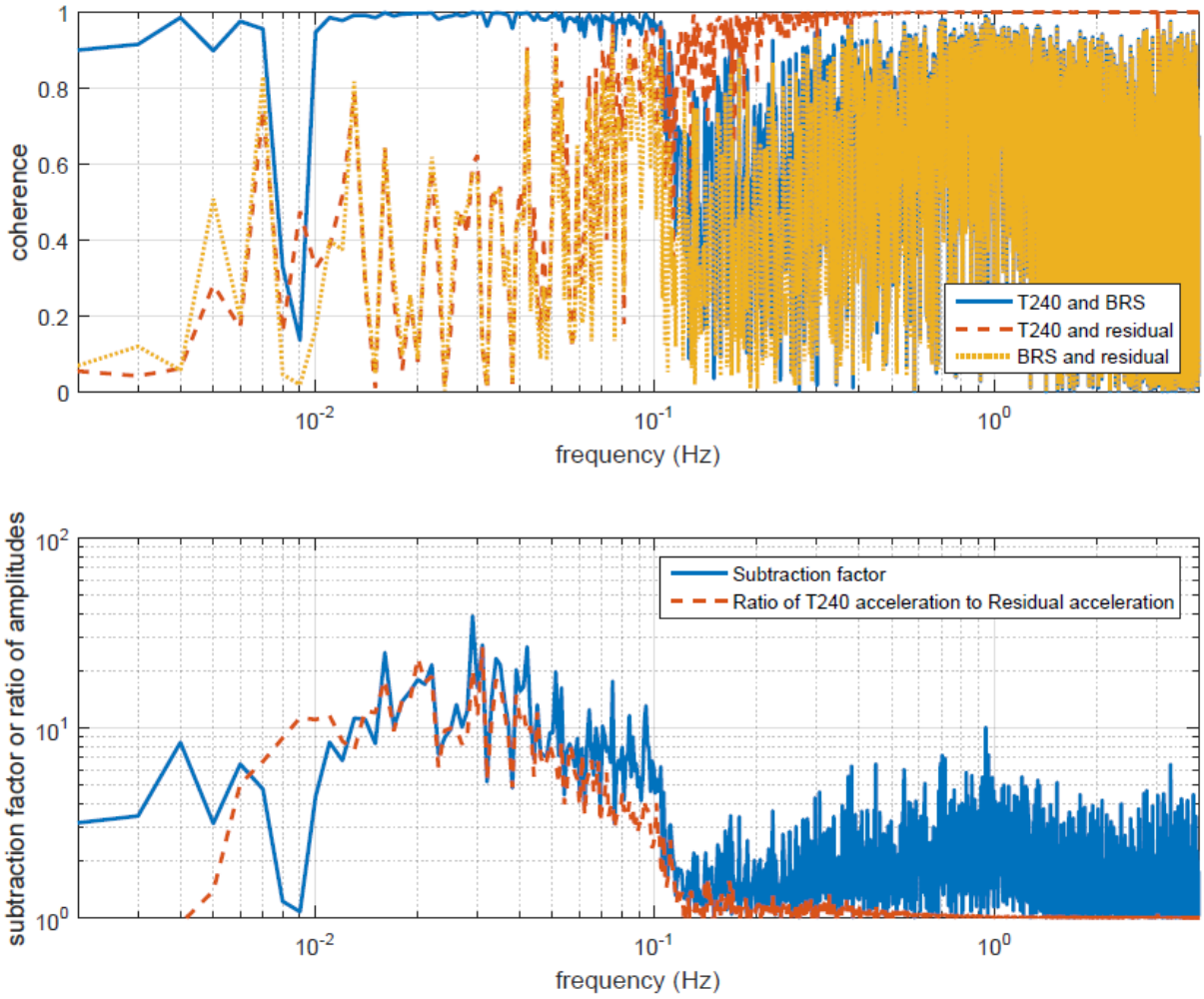

Figure 7: Coherence between T240, BRS and acceleration residuals, and the expected and measured subtraction factors.

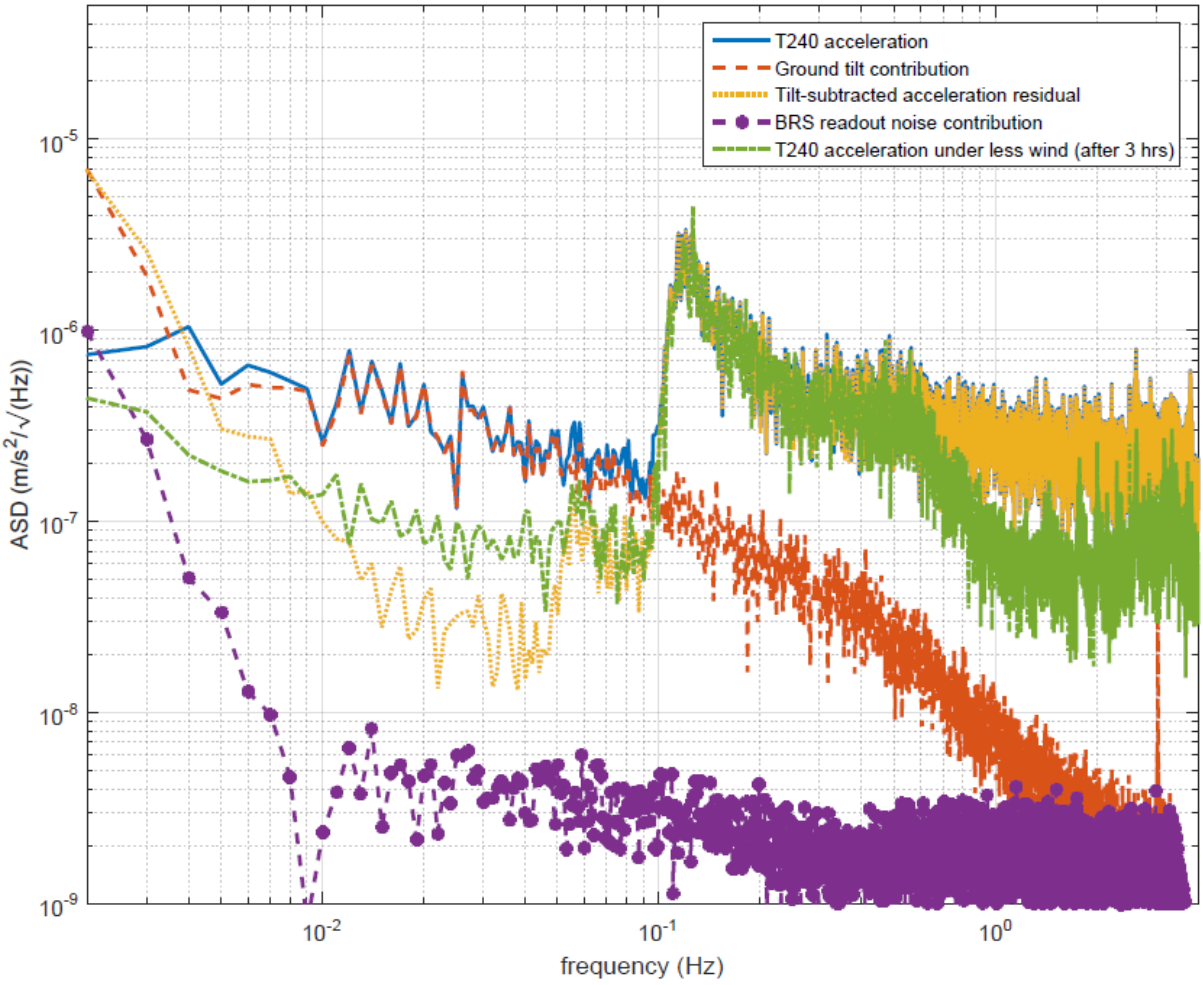

Figure 8: ASD and coherence of data under windy conditions on October 11 2014. The primary microseismic peak is visible after tilt-subtraction and is a consistent height over time.

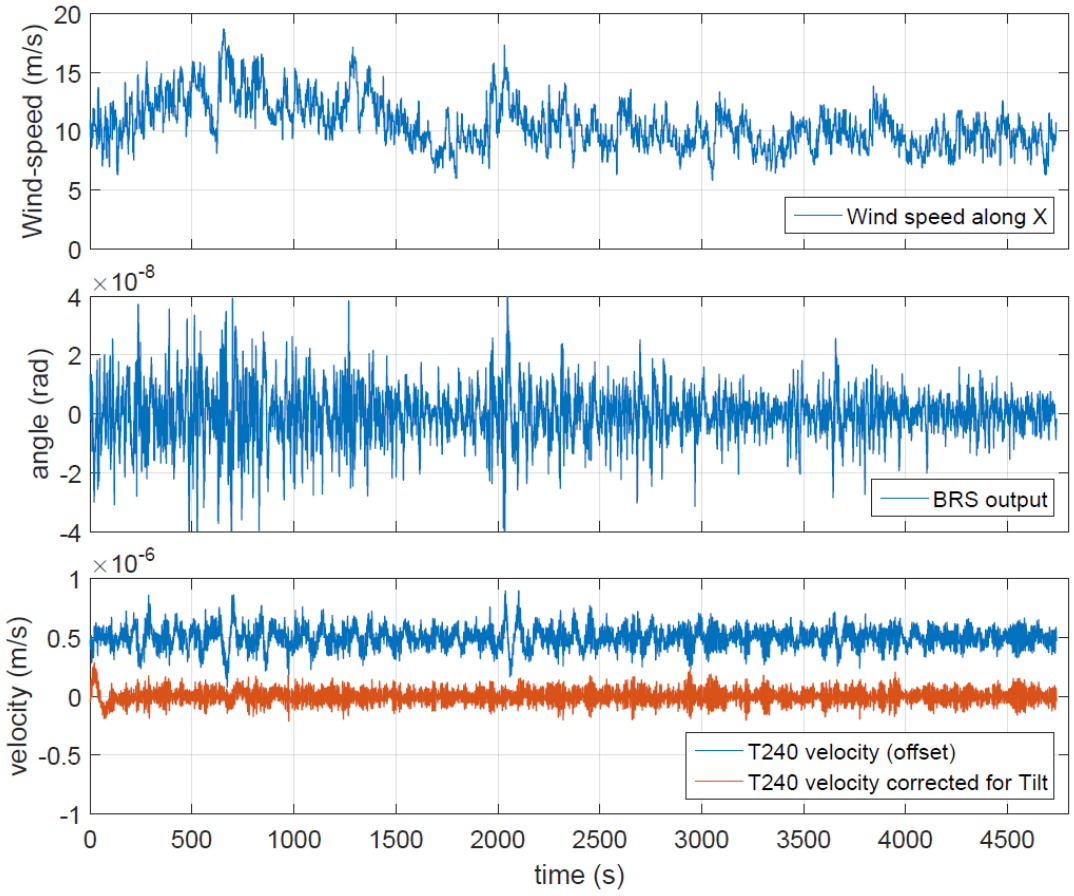

Figure 9: Time-series data from October 11 2014, starting at 00:45:00 UTC, showing a second high-wind duration.

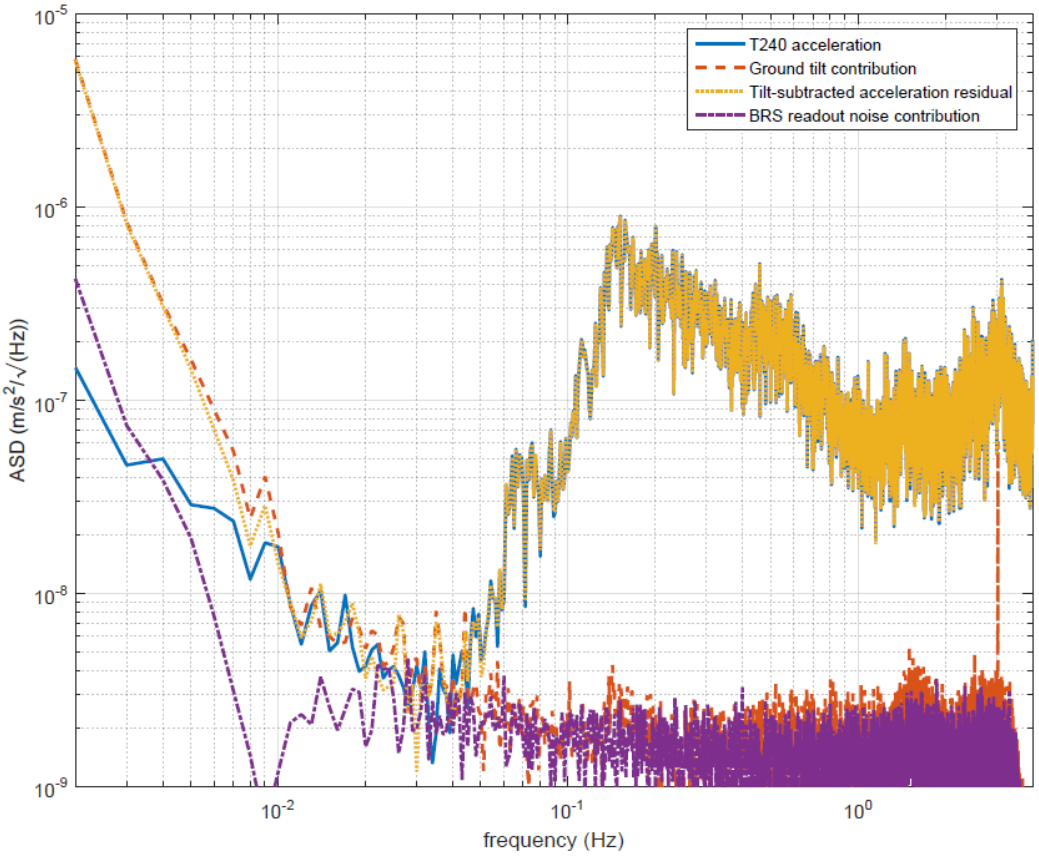

Figure 10: ASD and coherence of data during low wind-speeds on May 14 2015. This plot highlights the low translational sensitivity of the BRS by showing very small signals measured at the microseismic-peak frequency visible in the T240 acceleration.

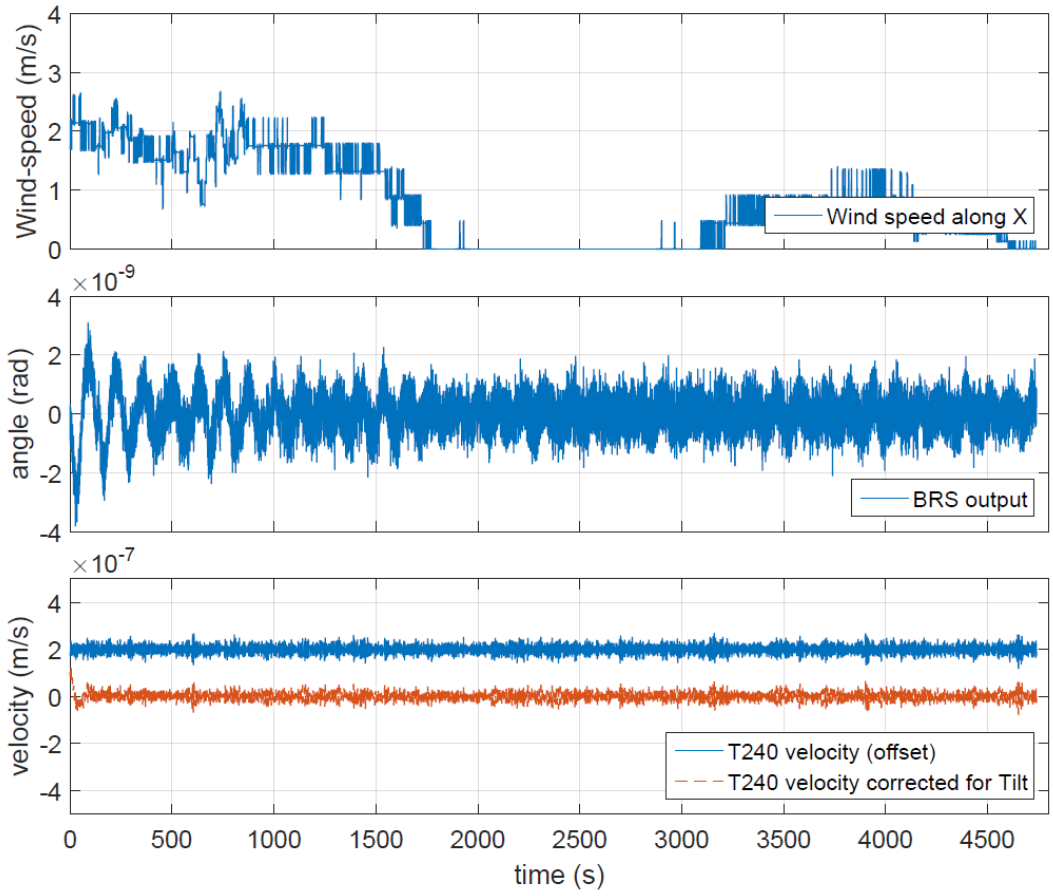

Figure 11: Time series data from May 14 2015, starting at 02:00:00 UTC, showing a low-wind duration.

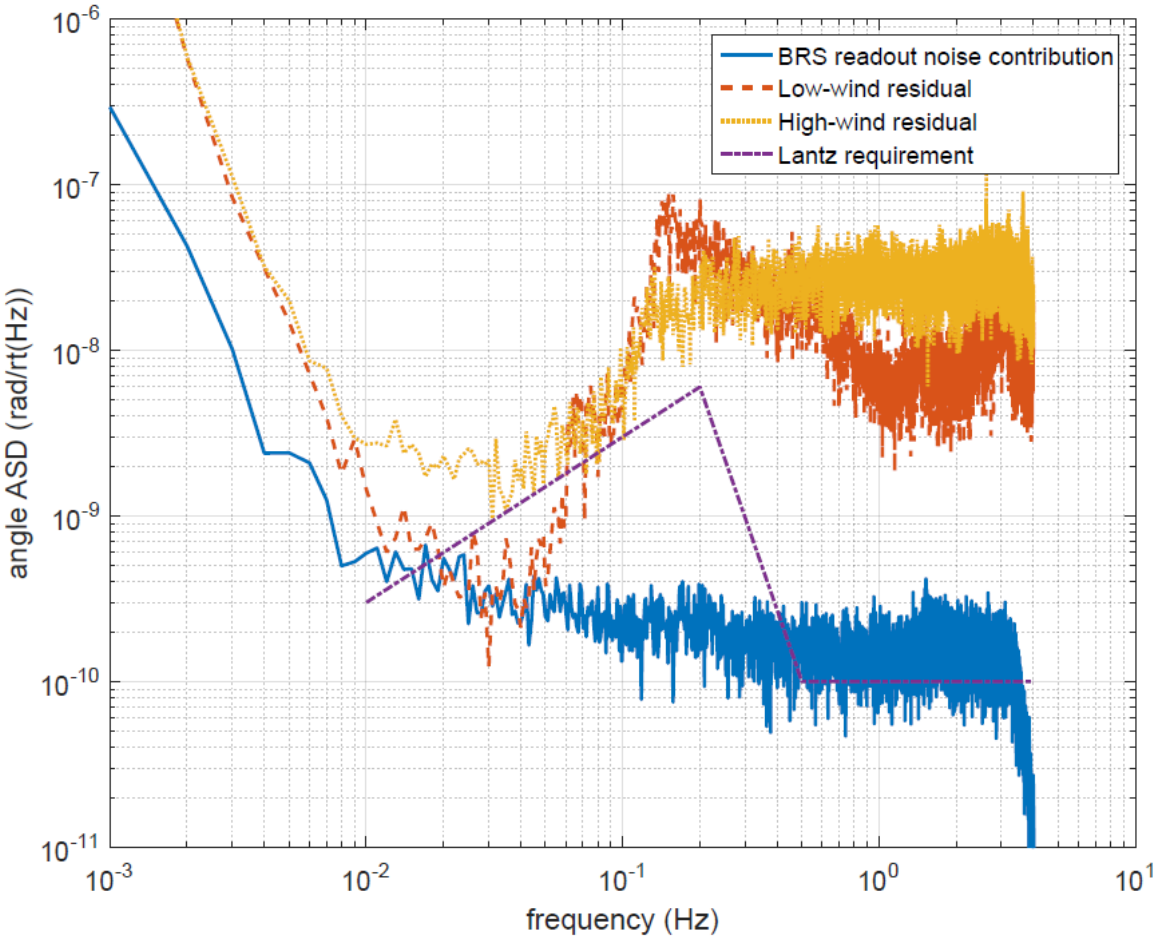

Figure 12: BRS readout noise contribution compared to the Lantz et. al. (2009) requirement. Also shown are the tilt-subtracted residual accelerations during low-wind and high-wind periods, converted to tilt units by dividing by *g*.

Appendix A: Equations of motion and tilt-subtraction

The torque on the beam-balance, as measured in the lab-frame can be expressed as

$$\tau = I\ddot{\theta}_a + \kappa(1 + i\varphi)\theta_a \qquad \text{(A1)}$$

where I is the moment of inertia and κ is the flexure torsional stiffness and φ is the flexure's intrinsic loss factor. It can be shown (**Venkateswara *et al*. (2014)**) that the measured torque is

$$\tau = \tau_{ext.} - I\ddot{\theta}_p - Mda_x \tag{A2}$$

where M is the total mass of the balance, d is the separation between the center of mass (COM) and the suspension point/pivot (d>0 if COM is below the pivot) and $a_x = \ddot{x} + g\theta_p$ is the horizontal acceleration at the pivot. Ignoring small corrections due to the location difference between the T240 and BRS, we assume that a_x is equal to the acceleration measured by the T240. $\tau_{ext.}$ is the sum of all external torques on the balance. This can include terms like Brownian-motion torques, torques from gravity gradients etc., which are usually quite small. The last two terms in the above equation can also be interpreted as the pseudo forces due to the non-inertial lab frame. This relation can be rewritten in frequency space as

$$-I\theta_a\omega^2 + I\theta_a\omega_0^2(1 + i\varphi) = \tau_{ext.} + I\theta_p\omega^2 + Md(g\theta_p - x\omega^2) \tag{A3}$$

where ω_0 is the resonance frequency of the beam-balance and we have retained the same symbols for the Fourier transforms of the original variables for convenience. Setting ground displacement to 0, the tilt-response of BRS in frequency-space is

$$\frac{Measured\ angle}{Input\ Angle} = \frac{\theta_a}{\theta_p} = \frac{\omega^2 - \omega_g^2}{\omega^2 - \omega_0^2(1 + i\varphi)} \tag{A4}$$

where $\omega_g = \sqrt{\frac{Mgd}{I}}$. The response is flat and unity at frequencies well above the resonance, goes to zero at ω_g and goes to a constant value at low frequencies. The high-frequency response ($\omega \gg \omega_0$) is due to the inertia of the balance, while the response at low frequencies ($\omega \ll \omega_0$) comes from its acceleration sensitivity (due to finite 'd'). The zero in the response, ω_g, is the frequency at which these two effects are equal and opposite.

The response to horizontal acceleration is given by

$$\frac{Measured\ Angle}{Input\ acceleration} = \frac{Md}{I}\frac{1}{\omega^2 - \omega_0^2(1+i\varphi)} \tag{A5}$$

Based on the above, one would like to design the balance such that 'd' is as small as possible in order to minimize acceleration coupling. In practice, it can be adjusted by measuring the driven-transfer function of the instrument and adding trim weights to the balance to make it small. For the BRS, d was about (33 +/- 5) micrometers.

To separate the horizontal acceleration measured by a seismometer into displacement and rotation components, we can use the fact that the seismometer measures the net horizontal acceleration, a_x, and express the ground rotation in terms of the BRS measurement, θ_a, and a_x. Using eq. (A3), the ground rotation w.r.t. an inertial frame can be expressed as

$$\theta_p = -\frac{\omega^2 - \omega_0^2(1+i\varphi)}{\omega^2}\theta_a + \frac{Md}{I\omega^2}a_x \tag{A6}$$

This 'inertial'-ground rotation (times g) can then be subtracted from a seismometer's acceleration, thus separating displacement and rotation.

Appendix B: Measurement of the Horizontal Translational Sensitivity of the Beam-Rotation-Sensor

The response of the beam-balance to horizontal acceleration is given in equation A3. Assuming that the horizontal acceleration is coming only from horizontal translation, this equation can also be expressed as:

$$\frac{Measured\ Angle}{Input\ translation} = \frac{Md}{I}\frac{\omega^2}{\omega^2 - \omega_0^2(1+i\varphi)} \quad \text{(B1)}$$

where I is the moment of inertia, M is the total mass of the balance, d is the separation between the center of mass (COM) and the suspension point/pivot, ω is the angular frequency, ω_0 is the resonant frequency of the beam-balance and φ is the internal loss factor of the flexure.

At frequencies much higher than the resonance frequency, Eq. B1 reduces to the ratio M*d/I. For d of ~33 μm, M=4.2 kg and I = 0.59 kg-m^2, this is equal to 2.3×10^{-4} rad/m. This means that to demonstrate this translation rejection, we need a shake table for which a drive of 10 μm produces rotations of much less than 2.3 nrad. This is not easy to implement.

As the BRS instrument referred to in the paper was in use at the LIGO Hanford Observatory, we opted to demonstrate the translation/acceleration rejection of such an instrument using one in our lab. The principle and design of the two instruments is nearly identical and the only significant difference is that the 'd' value for the one in our lab is ~10 μm, as compared to 33 μm for the BRS.

The rotation-sensor is clamped to a 10-cm-thick and 1.7-m by 1.5-m Aluminum plate, which sits on three rigid feet. We made a fairly good translational drive by elevating the platform on flexural feet consisting of I-beams (~30 cm tall) and driving it with a long cable and stepper motor as shown schematically in Fig. 13. Even so, the drive produced ~17 μm of horizontal motion amplitude as measured by an inductive position sensor and about 40 nrad of tilt motion amplitude as measured (at very low frequencies) by an AGI (Applied Geomechanics Inc.) Model 755 tiltmeter. Thus, to obtain the translation response of the rotation-sensor, the response to this tilt was compensated. The residual after compensation is consistent with a d of 10 μm as shown

in Figure 14, but is not sensitive enough to confirm it. This measurement can also be reinterpreted to show the response to the applied horizontal acceleration as shown in Figure 15. In comparison, the response of the AGI tiltmeter is shown in Figure 16, which shows the expected (g/ω^2) dependence from acceleration coupling at high frequencies.

These measurements show the low translational sensitivity of the rotation-sensor, but cannot directly confirm the true translational sensitivity, due to the small tilt-systematic present in the drive.

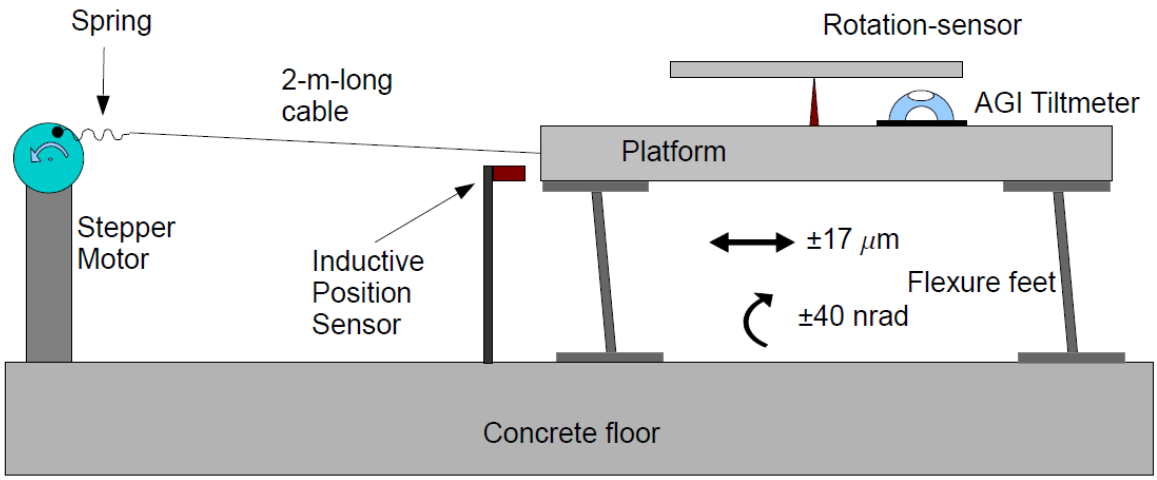

Figure 13: Shake Test Schematic. The spring is attached to an off-center-mounted bearing, which converts the rotary motion of the stepper in to a smooth sinusoidal force on the platform. The flexure feet enforce a large translation with minimal tilt.

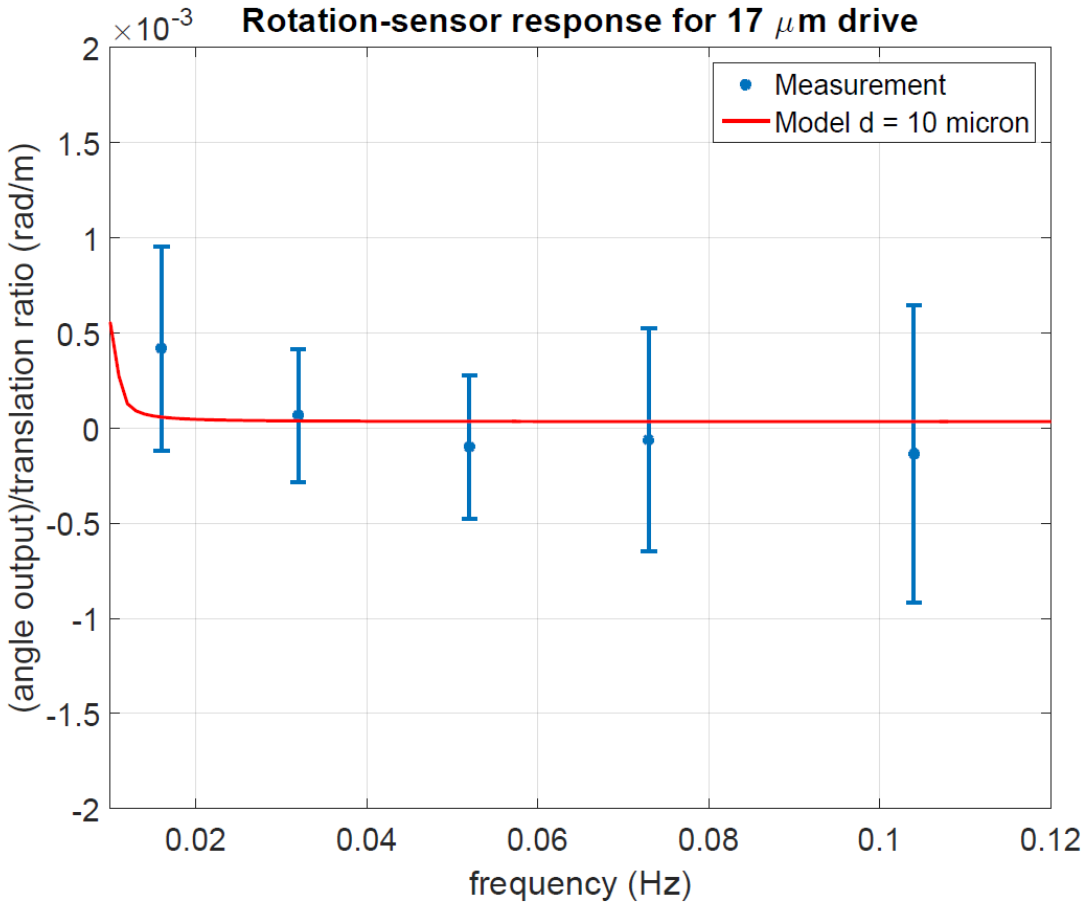

Figure 14: Rotation-sensor's response to horizontal translation. After compensating for the small tilt (as sensed by the independent AGI tiltmeter), the residual response is consistent with the model and confirms that it is very small.

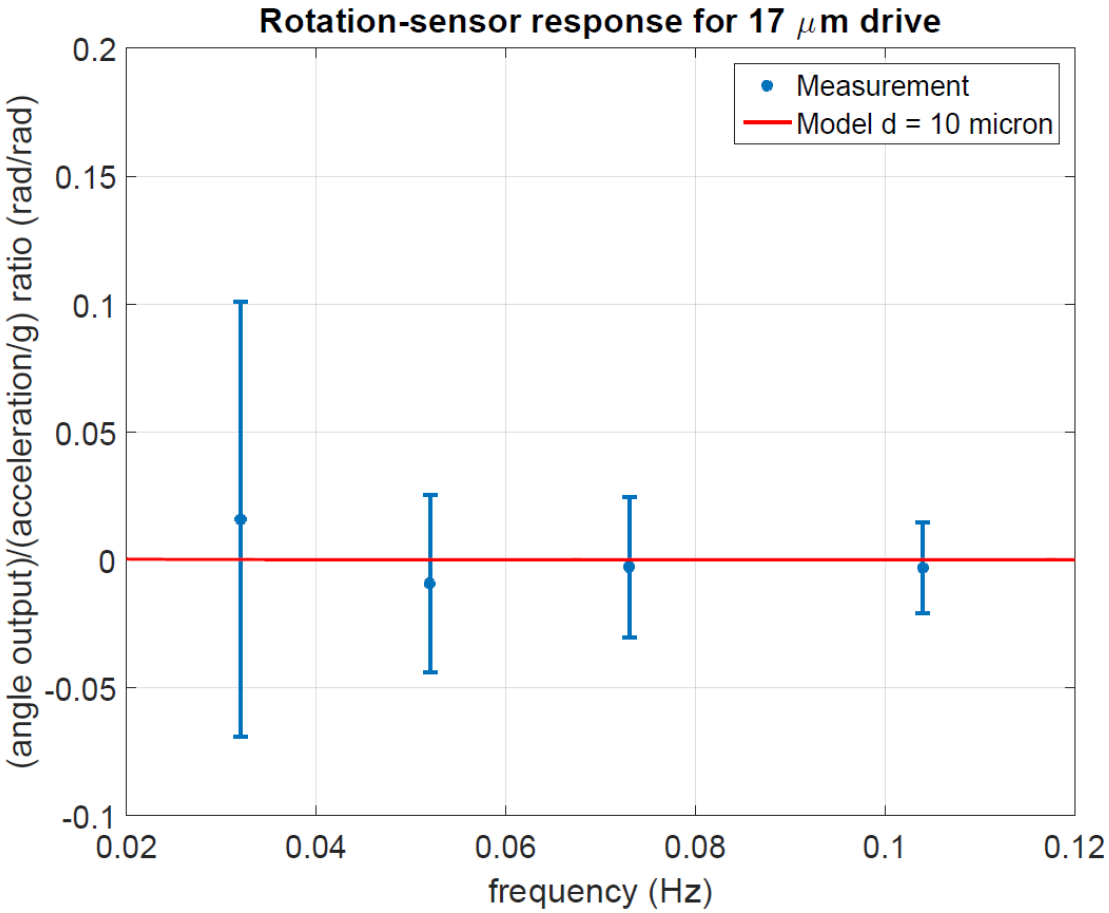

Figure 15: Rotation-sensor's response to horizontal acceleration. Note that as the drive was constant in displacement, the acceleration signal was smaller at lower frequencies. Hence the errors in the ratio were larger at lower frequencies. The measurement confirms that the acceleration response is very small.

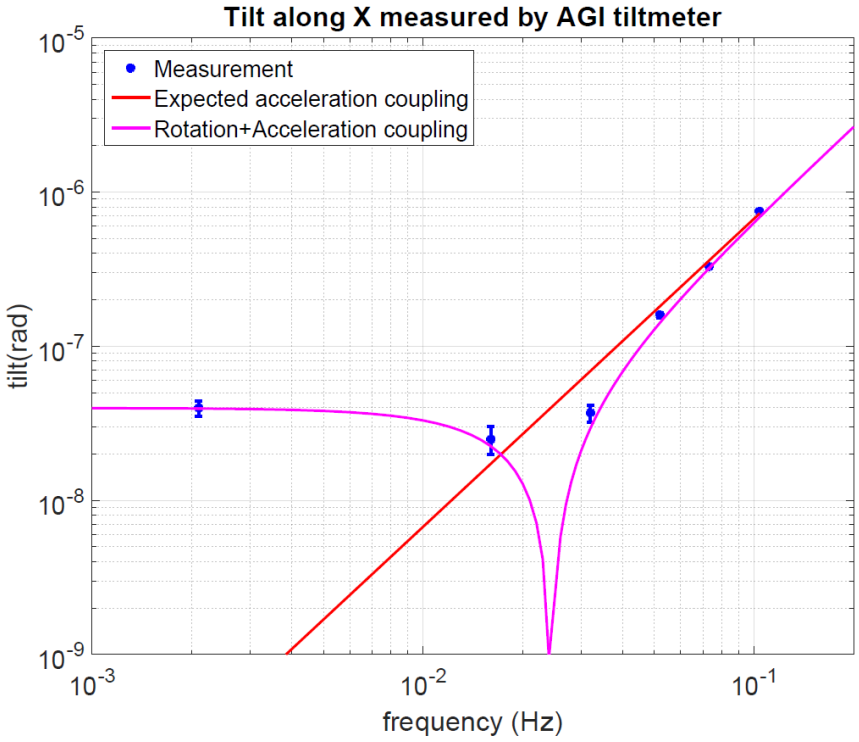

Figure 16: AGI-Tiltmeter's response to horizontal translation of 17 μm. At low frequencies, the response to the tilt of the table is visible. At higher frequencies, the response to the acceleration from translation was dominant.